This is a peer-reviewed, accepted author manuscript of the following research article: Tang, Y., Cai, Y., Wang, L., & Luo, X. (2022). Formation mechanism of superhydrophobicity of stainless steel by laser-assisted decomposition of stearic acid and its corrosion resistance. *Optics and Laser Technology*, *153*, [108190]. https://doi.org/10.1016/j.optlastec.2022.108190

Formation Mechanism of Superhydrophobicity of Stainless Steel by Laser-assisted Decomposition of Stearic Acid and its Corrosion Resistance

Yiping Tang[a,b,c], Yukui Cai[a,b,c*], Lei Wang[d*], Xichun Luo[e], Bing Wang[a, c], Qinghua Song[a, c], Zhanqiang Liu[a, c]

[a] School of Mechanical Engineering, Shandong University, Jinan, 250061, China;

[b] Shenzhen Research Institute of Shandong University;

[c] Key Laboratory of High Efficiency and Clean Mechanical Manufacture of MOE / National Demonstration Center for Experimental Mechanical Engineering Education at Shandong University;

[d] Department of Orthodontics, Qilu Hospital of Shandong University;

[e] DMEM, University of Strathclyde

ABSTRACT

Superhydrophobic surfaces have attracted extensive attention over the past decade, primarily due to their self-cleaning, corrosion resistance and anti-bacterial abilities. However, it is still a challenge to prepare superhydrophobic surfaces with good chemical stability, low cost, environmental friendliness, and suitable for large-scale production applications. In this paper, a hybrid laser-chemical method to prepare superhydrophobic micro-patterns on 316L stainless steel were put forward, which combined laser ablation and laser assisted chemical decomposition of stearic acid ($C_{17}H_{35}COOH$). Experiments show that under the laser power of 10 W, the frequency of 150 kHz, the speed of 20 mm/s, and the mesh spacing of 75 μm, the best superhydrophobicity with a static contact angle of 153.9° can be obtained. The fundamental mechanism of laser-chemical method is the increase of the non-polar C-C(H) bond of specimen by laser assisted hydrodeoxygenation reaction of stearic acid. Moreover, unlike laser ablation-stearic acid coated specimen, the specimen prepared by laser-chemical method can maintain superhydrophobicity after 10 minutes of ultrasonic cleaning. The electrochemical corrosion experiments shows that the hybrid laser-chemical method can manufacture superhydrophobic specimens with better chemical durability and corrosion resistance.

Keywords: Laser-chemical method; Superhydrophobic surface; Stearic acid; Corrosion resistance

1. Introduction

In recent years, 316L stainless steel has a wide range of applications in various

fields because of its good corrosion resistance. However, it is a hydrophilic material (static contact angle is less than 90°). Corrosion is still a serious problem faced by stainless steel materials during safe service. For example, 316L stainless steel is mainly used to make orthodontic brackets, arch wires, denture brackets, and jaw splints in the oral medical. Human saliva may cause corrosion of stainless steel, accelerate the release of metal ions and cause severe allergic reactions. In addition, 316L stainless steel also widely used in marine engineering equipment, aerospace and other fields. Stainless steel electrical connectors are corroded in the marine salt spray environment, which greatly affects the reliability of the electrical power. Hence, enhancing the corrosion resistance of 316L stainless steel by constructing a superhydrophobic surface is of great significance for increasing the service life of these equipment.

Natural biological surfaces, such as lotus leaf, rice leaf, rose petal, dragonfly and butterfly wings have attracted so much attention over the last few decades. It is mainly due to their hydrophobicity that formed during long-time evolution and natural selection. Generally, a superhydrophobic surface refers to a surface with a minimum water static contact angle of about 150° and a sliding angle of no more than 10° [1-2]. Lotus leaf is a natural product with superhydrophobicity, which has a "self-cleaning" effect to avoids dust pollution [3-4]. This is mainly due to its micro-nano structure and wax with low surface energy. Hence, artificial superhydrophobic surfaces, usually created by surface structuring or coating technology, have received tremendous attention in recent years. Superhydrophobic surface has been successfully applied in various fields, including water transfer, corrosion resistance, anti-icing, self-cleaning, abrasion resistance, drag reduction and biomedical applications [5-6]. Surface chemical composition and morphology are two critical factors in determining their hydrophobicity [7-8]. Therefore, it is possible to make a rough surface containing micro-nano structures and then modify it by introducing materials with low surface energy (such as fluoroalkyl silane and lauric acid) to obtain a super-hydrophobic characteristic [9-10]. Previous studies have shown that methods such as electrochemical deposition, chemical vapor deposition, wet chemical reaction lithography, and solution immersion method can be used to successfully prepare superhydrophobic surfaces [11-14]. The surface produced by chemical methods may indeed exhibit good superhydrophobicity, but usually has low stability and short service life. The low production efficiency and high cost of superhydrophobic surfaces are the primary challenges restricting its industrial application [15].

Compared with chemical methods, the laser ablation process is a reliable manufacturing method due to its high-efficiency and contactless characteristics. Normally, femtosecond, picosecond or nanosecond lasers can be employed to prepare micro-nano structures on different materials. However, most metal materials have an intrinsic hydrophilic property, the laser ablated specimen require further post-treatment process to obtain superhydrophobicity.

Currently, three different post-processes are put forward to realize the superhydrophobicity of laser ablated specimens and can be summarized as follows.

First method is additional heat treatment after laser ablation process. Ph.D. Ngo et al. [16] prepared micro-nano structures on the titanium by nanosecond pulsed laser, and processed at a high temperature of 200°C for 6 hours to obtain a superhydrophobic surface with a contact angle of 168°. The EDS test results proved that the carbon content on the surface after high-temperature treatment is significantly increased, and the surface energy is effectively reduced. The above method is also suitable for the preparation of superhydrophobic surfaces of aluminum alloy, stainless steel and copper [17-19]. However, the obtained superhydrophobic surface has low thermal stability and poor durability.

The second method is to put the laser ablated surface in ambient air to absorb organic matter. Vanitha et al. [20] used nanosecond pulsed laser prepared specimens with different line spacing on titanium surface. Initially, the structured laser patterned surfaces with dual scale roughness were hydrophilic. With the increase of storage time in ambient conditions of the sample, the contact angle slowly increases to 160° due to the accumulation of atmospheric hydrocarbon compounds on the surface. Van-Duong et al. [21] employed nanosecond laser to process micro-nano structures on 304 stainless steel and copper, and found that it takes 13 days for 304L stainless steel to transform from hydrophilic to superhydrophobic, while copper requires 11 days. Tian et al. [22-23] found that aluminum and GH1469 nickel-based alloys can be transformed from hydrophilic to superhydrophobic within 30 days after nanosecond laser ablation. However, the ageing method has a longer preparation period and lower manufacturing efficiency, which is not convenient for large-scale production of superhydrophobic surfaces.

The third most commonly used method is to use low surface energy chemical reagent such as silane to coating the surface. Mazumder et al. [24] prepared micro-nano structure on 316L stainless steel by femtosecond laser, and then coated trichlorosilane on the surface of the micro-nano structure by chemical vapor deposition to obtain a superhydrophobic surface with a maximum contact angle of 150°. Moradi et al. [25] and Jagdheesh et al. [26] used a method that combined femtosecond or picosecond laser ablation with fluorosilane modification to prepare superhydrophobic surfaces on stainless steel, titanium alloy and aluminum alloy. Bai et al. [27] employed femtosecond laser to manufacture microgroove arrays on the shape-memory polymer substrates. The groove-structured surface exhibited superhydrophobicity and anisotropic wettability after fluoroalkyl silane modification. However, fluorosilane can result in serious environmental pollution, which has long-lasting environmental stability and high bioaccumulation. These reagents have been banned and listed on the United Nations list of organic pollutants. Moreover, these laser-based multistep preparation methods have disadvantage of low efficiency, high cost. Therefore, the development of environmental-friendly and high efficiency laser-based process is critical to manufacture superhydrophobic surface for large scale metal components.

Many scholars pay attention to the corrosion resistance of superhydrophobic surfaces. Lu et al. [28] used ultraviolet nanosecond laser to process superhydrophobic

surface on 316L stainless steel, and evaluated the corrosion resistance by PDP, found that the surface corrosion current density (I_{corr}) decreased by two orders of magnitude. Qian et al. [29] used a picosecond laser to fabricate a superhydrophobic surface on nickel-aluminum bronze. The electrochemical corrosion results showed that the corrosion resistance of NAB was improved when the scanning distance was less than 80 μm. Similarly, the research of Lara et al. [30] and Ludmila et al. [31] both showed that the corrosion resistance of the aluminum alloy superhydrophobic surface obtained by different preparation methods has been improved.

This paper proposed a hybrid laser-chemical method to prepare superhydrophobic surface with advantage of environmentally friendly and high efficiency. Firstly, this method employed nanosecond pulsed laser to obtain micro-patterns, then stearic acid (a commonly used environmentally friendly and inexpensive hydrocarbon) as a chemical modifier were coated on the laser ablated specimen. Thirdly, secondary laser ablation process to induce the decomposition of coated stearic acid and realize the reduction of surface energy. Furtherly, the laser ablation parameters and surface pattern are optimized through experiments to achieve specimens with better superhydrophobicity. Then the formation mechanism of superhydrophobicity was investigated. Lastly, the comparison of chemical durability and corrosion resistance of specimens prepared by different manufacturing processes were investigated. The study proved that hybrid laser-chemical process can prepare metal superhydrophobic surfaces with high efficiency, low cost, and low pollution. A three-step machining process can be integrated into one laser machining machine with only one workpiece clamping, it has a broad application prospect in the industrial field in the future.

2. Methodology

2.1 Materials

As-received 316L sheets (Shanghai Ranshan Metal Materials Co., Ltd.) with chemical composition shown in Table 1 were cut into 10×10×2 mm^3 as substrates. These samples were used throughout the research process. Ethanol and acetone (analytical reagents, 99%) are used to clean the surface and remove contaminants attached to the surface. Stearic acid is used as an agent for reducing surface energy. The chemical reagents in this study were purchased from Guangzhou Chemical Reagent Co., Ltd., China.

Table 1 Mass fraction of elements in 316L wt.%.

Elements	Fe	Cr	Ni	Si	C
Mass fraction	67.93	16.53	14.36	1.15	0.03

2.2 Hybrid laser-chemical process

The schematic of laser-chemical process is shown in Fig. 1. The nanosecond pulsed fiber laser parameters are shown in Table 2. First of all, nanosecond laser was employed to manufacture micro-patterns on 316L stainless steel specimen, and specimens was cleaned ultrasonically with acetone and ethanol for 5 minutes. Then, an

ultrasonic atomizer was used to produce micro drops from stearic acid of the ethanol solution，the mass fraction is 3% and the spraying time is 3 minutes. Once the ethanol evaporates, micro particles of stearic acid will remain on the surface. Lastly, nanosecond pulsed laser irradiates the surface again to assist the decomposition of stearic acid. All specimens were cleaned ultrasonically with deionized water, acetone and ethanol for 5 minutes respectively to remove residual organics on the surface.

Table 2 Parameters of nanosecond fiber laser.

Laser parameters	Maximum output power	Wavelength	Pulse width	Maximum Repetition rate	Spot diameter
Value	20 W	1064 nm	100 ns	200 kHz	30 μm

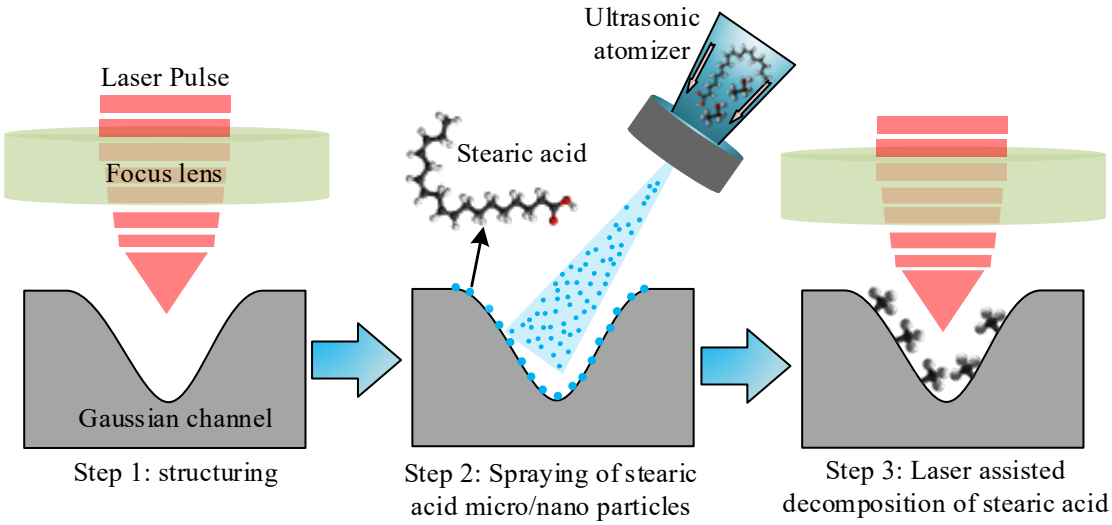

Fig. 1. Schematic of laser-chemical process

2.3 Experimental setup

In this research, single factor experiments were designed to investigate the effect of laser ablation parameters for Step 1 and Step 3, then the third experiment aims to optimize pattern type and spacing of micro-patterns based on optimized laser ablation parameters of Step 1 and Step 3. The nanosecond pulsed laser texturing system and the corresponding laser scanning strategies are schematically shown in Fig. 2.

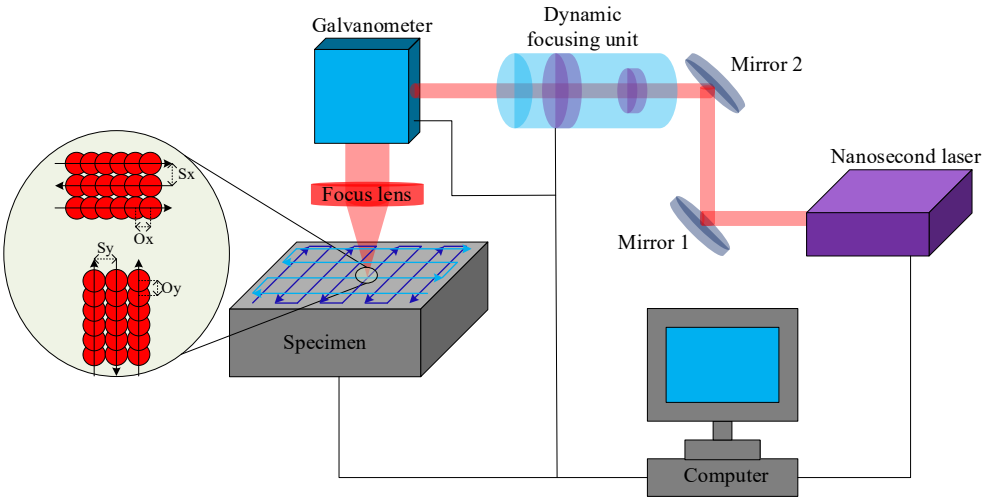

Fig. 2. Schematic of nanosecond pulsed laser texturing system and laser scanning strategies

Table 3 and Table 4 show the details of the operational conditions used to optimize laser ablation parameters for Step 1 and step 3, respectively. In Experiment 1, varied laser ablation parameters were used for Step 1 and the laser power for Step 3 is constant as 2 W. In Experiment 2, varied laser ablation parameters for Step 3 were used and Step 1 used the best parameters in experiment 1.

Table 3 Experiment 1: operational conditions used to optimize laser parameters for Step 1

Specimen No.	Power for step 1 (W)	Frequency for step 1 (kHz)	Scanning speed for step 1 (mm/s)	Spacing for step 1 (μm)	Pattern type for step1
1	5	50	20	50	Mesh
2	5	100	20	50	Mesh
3	5	150	20	50	Mesh
4	5	200	20	50	Mesh
5	10	50	20	50	Mesh
6	10	100	20	50	Mesh
7	10	150	20	50	Mesh
8	10	200	20	50	Mesh
9	15	50	20	50	Mesh
10	15	100	20	50	Mesh
11	15	150	20	50	Mesh
12	15	200	20	50	Mesh
13	20	50	20	50	Mesh
14	20	100	20	50	Mesh
15	20	150	20	50	Mesh
16	20	200	20	50	Mesh

Table 4 Experiment 2: operational conditions used to optimize laser parameters for Step 3

Specimen No.	Power for step 3	Frequency for step 3	Scanning speed for step 3	Spacing for step 3	Pattern type for step 3

	(W)	(kHz)	(mm/s)	(μm)	
S1	1	150	50	50	Mesh
S2	2	150	50	50	Mesh
S3	3	150	50	50	Mesh
S4	4	150	50	50	Mesh
S5	5	150	50	50	Mesh

Specimens with different patterns and spacing, as shown in Table 5, are prepared based on the optimized laser processing parameters in Experiment 1 and Experiment 2.

Table 5 Experiment 3: optimization of pattern type and spacing of micro-patterns.

Specimen No.	Spacing for step 1 and 3 (μm)	Pattern type for step 1 and 3
L1	25	Grooves
L2	50	Grooves
L3	75	Grooves
L4	100	Grooves
L5	125	Grooves
L6	150	Grooves
W1	25	Mesh
W2	50	Mesh
W3	75	Mesh
W4	100	Mesh
W5	125	Mesh
W6	150	Mesh

2.4 Characterization

A scanning confocal microscope (CLSM, Keyence, Osaka, Japan) were employed to observe the surface morphology of laser ablated specimens, and then put it into an emission scanning electron microscope (SEM, Zeiss, Germany) and an energy spectrometer (EDS, Oxford Instruments, UK) to examine the micro-nano surface structure and element composition. A contact angle measuring instrument (JC2000A, Powereach, China) to evaluate the superhydrophobicity of the specimen, and take five measurements at different positions on the surface to get the average value to avoid potential errors in any one measurement. X-ray photoelectron spectroscopy (XPS, Escalab 250Xi, USA) was used to analyze the chemical state of the surface.

3. Results and discussion

3.1 Effect of laser ablation parameters on superhydrophobicity

The experiments as shown in Table 3 aims to investigate the influence of different laser power and pulse frequency on the wettability of laser ablated surfaces during the Step 1. Fig. 3 shows the variation trend of contact angle at different laser power and pulse repetition frequency for Step 1. Specimen prepared by laser ablation process showed superhydrophilicity with a contact angle of 15.4°. However, for the specimen prepared by laser-chemical process, the contact angle is increased apparently. When the

laser processing power is 5 W, few materials are removed from the surface of the specimen, and the formed micro-nano structure size is small, hence a higher contact angle cannot be obtained. Under the power of 10 W, when the frequency is increased from 50 kHz to 150 kHz, the contact angle increased continuously from 139.3° to 146.9°. However, further increase of pulse repetition frequency and power to 15 W or 20 W result in a decrease of contact angle. At low frequency (50 kHz) or high power (15 W, 20 W), the laser energy density is too high, the material removal rate is high, the processing heat effect is significant, and the melt flow of residue and material makes it difficult to guarantee the uniformity of the micro-patterns, which is not conducive to superhydrophobic gas. The formation of cavities thus leads to a decrease in the contact angle. As a result, the optimized laser ablation parameters for Step 1 is 10 W for laser power and 150 kHz for pulse frequency, the contact angle of 146.9° can be obtained.

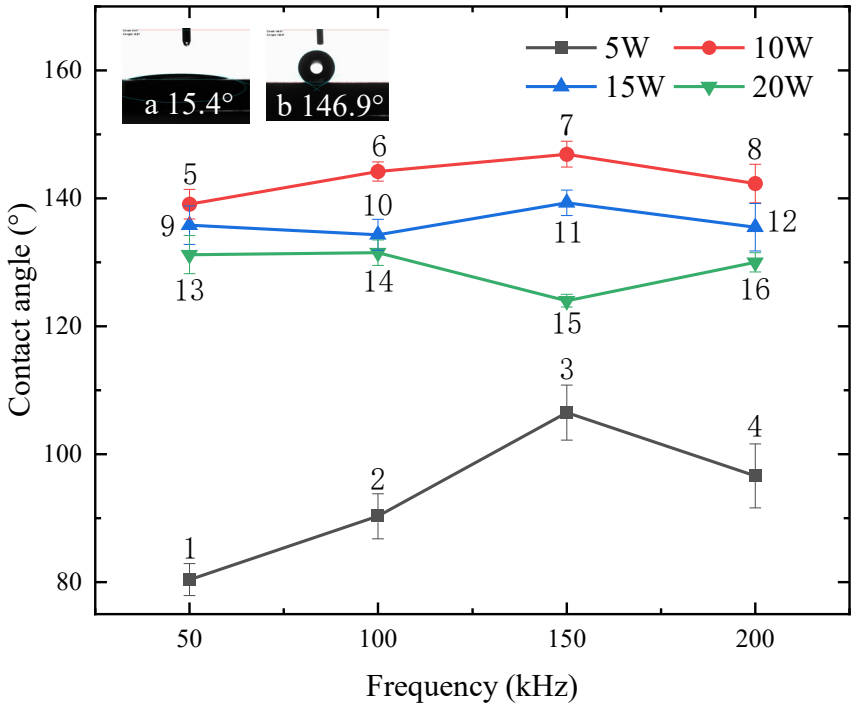

Fig. 3. Variation of contact angle at different laser power and frequency for Step 1 in Experiment 1; [a] Specimen prepared by laser ablation method (10 W, 150 kHz), [b] Specimen prepared by Laser-chemical method (Specimen No.7).

The experimental results for optimization of Step 3 are shown in Fig. 4. When the power is 1 W, the specimen has a contact angle of 148.3°. However, with the increase of laser power, the contact angle shows a decreasing trend. When the laser power for step 3 is chosen as 5 W, black smoke was generated on the surface of the specimen in the experiment, and stearic acid was mostly vaporized and carbonized, the specimen only has a contact angle of 80.8°. Hence, chose a smaller laser power in Step 3 is critical for the thermal decomposition of stearic acid and the reduction of surface energy.

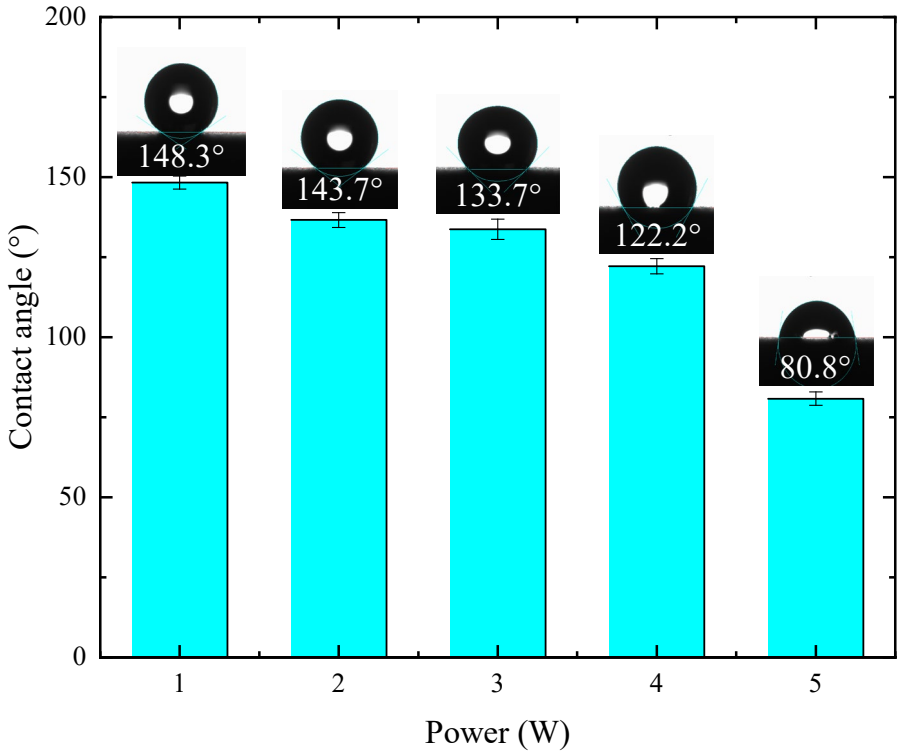

Fig. 4. Contact angle for different laser power in Step 3

3.2 Effect of surface pattern and structure dimensions on superhydrophobicity

Under the irradiation of the laser pulses, the machined surface is ablated or gasified because of the huge heat generated. The machined surface is spattered, and a large number of spattered melts accumulate with each other to form a bulge on the surface. With the movement of the laser beam, the ablation area rapidly settles, cools and solidifies. Fig. 5 (a) and (b) shows the SEM images of surface and section of laser processing with a line spacing of 50 μm. Grooves, corrugated protrusions and spherical particle structures can be seen on the surface and section. This formation is an iterative dynamic process including melting, evaporation, etching, re-solidification and ablation. When the laser energy density exceeds the melting threshold of stainless steel, melting and vaporization occur in the irradiated area, and then solidify rapidly as the laser spot moves away. Due to the Gaussian intensity distribution of the laser spot, the energy density at the center of the circular spot is higher than that at the edge, resulting in a temperature gradient in the irradiated area. Micro-protrusions are created due to surface tension and temperature gradients [32-33]. At the same time, some of the melt in the center was moved to the edges due to the temperature gradient. Finally, ridge-like micro-patterns were produced.

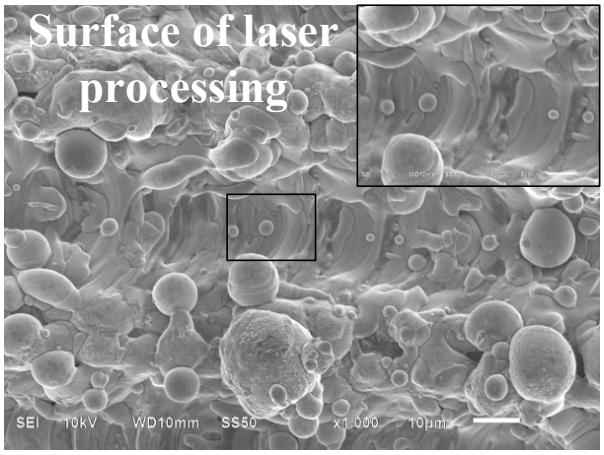

(a) SEM images of laser processing surface

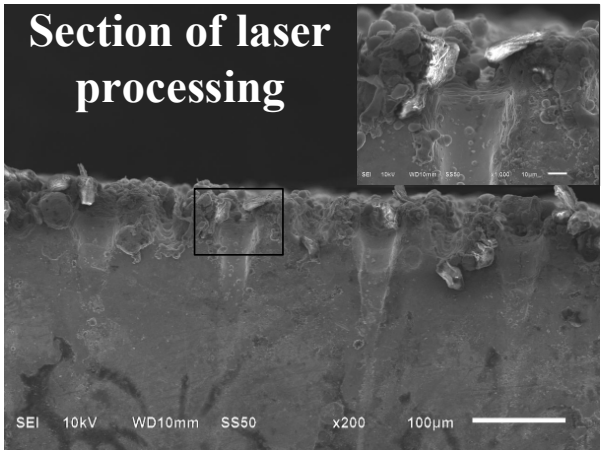

(b) SEM images of laser processing section

Fig. 5. SEM images of laser processing surface (a) and section (b)

The spacing and type of micro-patterns on the laser processing surface has a significant effect on the water contact angle. Using the optimal laser parameters optimized in Experiment 1 and Experiment 2, the laser-chemical processing was performed on the stainless steel surface by changing the scanning path and spacing of the laser. Fig. 6 (a) shows the surface morphologies of the grooves and mesh patterns with different pitches (25 μm, 50 μm, 75 μm, 100 μm, 125 μm, 150 μm). Both the grooves and the mesh pattern form a regular bulge when the spacing is great than 75 μm, With the spacing increases, the grooves surface gradually forms a stripe structure, the edge accumulation around the mesh surface and form square groove structures. When the spacing is smaller than 75 μm, the overlap rate of laser beam is high, and the surface melt is overlapped after accumulation, so the groove structure cannot be formed. Fig. 6 (b) displayed the variation of contact angle for different specimens. Seen from that, a continuous increase in contact angle, namely from 146.9° to 153.9°, occurs as the spacing increases from 25 μm to 75 μm. However, further increase beyond this spacing result in decreasing of contact angle. Hence, the results indicate that the laser textured stainless steel surface exhibited best hydrophobicity when the spacing is 75 μm, where the corresponding contact angle is about 153.9°. Furthermore, under the

same spacing, the specimen with mesh patterns display better superhydrophobicity than the surface with grooves.

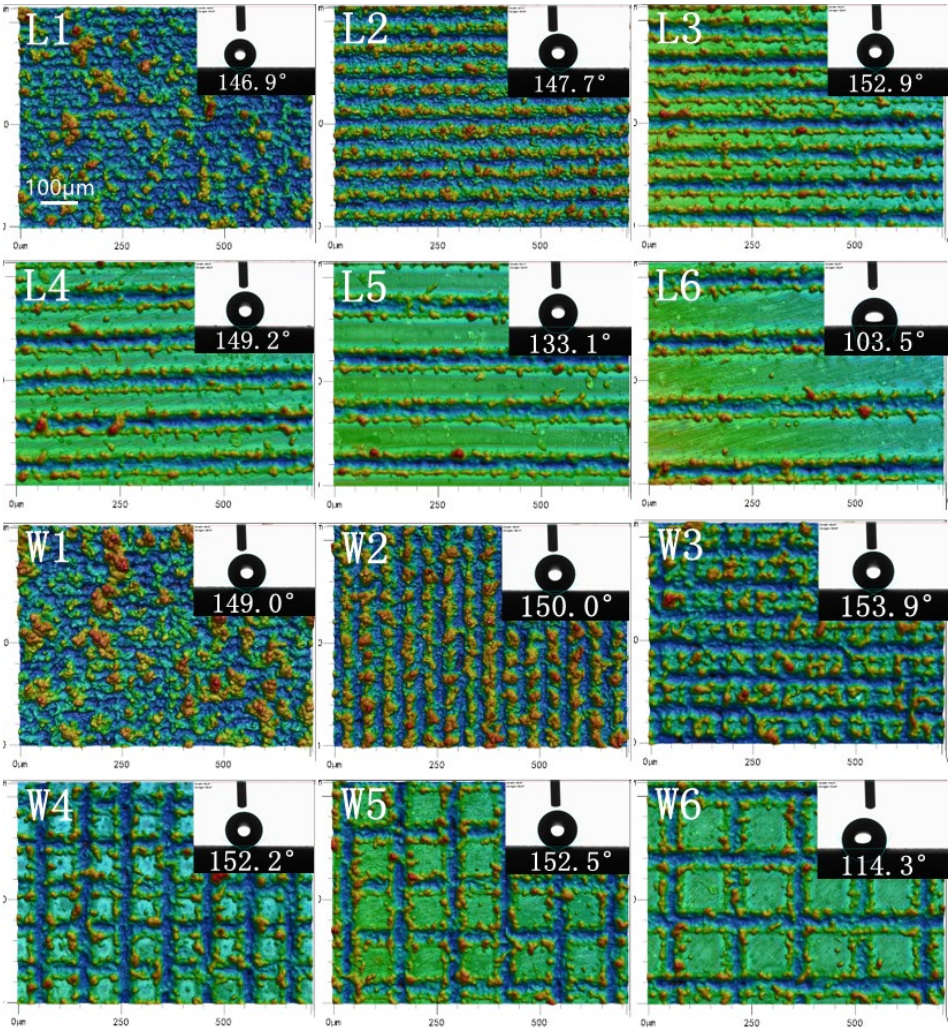

(a) Surface morphologies micro-patterns at different spacing

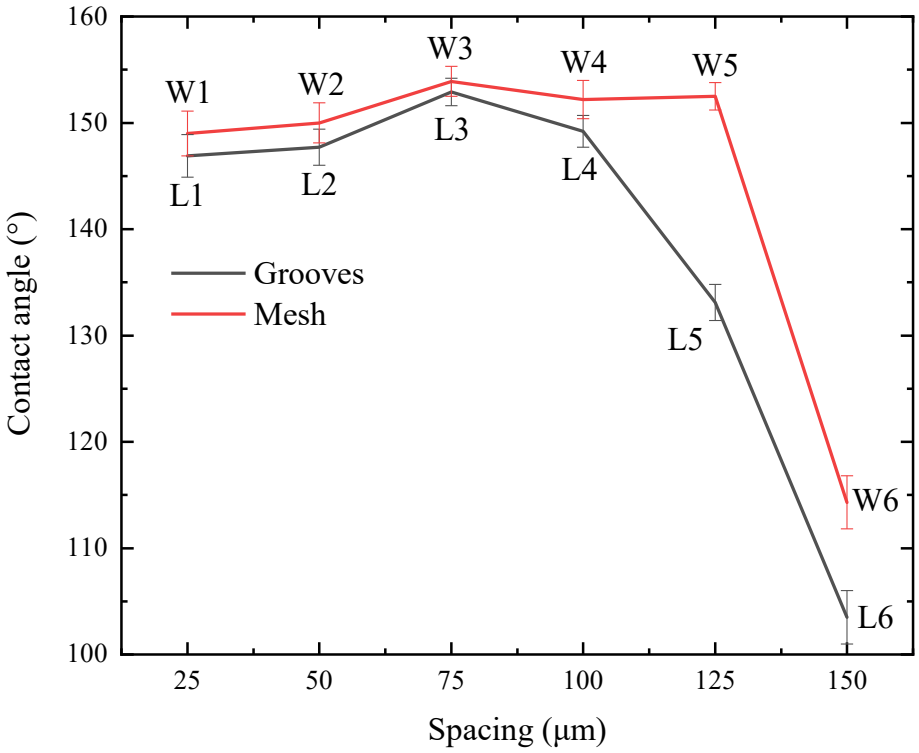

(b) The variation of contact angle for different specimens

Fig. 6. Surface morphologies (a) and contact angles (b) of grooves and mesh micro-patterns at different spacing. (Grooves:L1 25 μm、L2 50 μm、L3 75 μm、L4 100 μm、L5 125 μm、L6 150 μm. Mesh: W1 25 μm、W2 50 μm、W3 75 μm、W4 100 μm、W5 125 μm、W6 150 μm).

3.3 Formation mechanism of superhydrophobicity of laser-chemical processed specimens

As shown in Fig. 7, the chemical composition of the laser processed surface and the laser-chemical processed surface W3(mesh patterns with spacing of 75 μm) was analyzed by EDS. Compared with laser processing specimen, the specimen prepared by the laser-chemical process has a higher carbon content, which increased from 1.62% to 10.47%. It is seen that stearic acid is essential to provide low surface energy in surface wettability. What's more, the oxygen is mainly associated with iron oxide, which is mainly derived from the laser ablation process. The weight percentage of oxygen after laser processing is 28.84%, which is higher than the superhydrophobic surface of the laser-chemical processing. It can be seen that surfaces modified with stearic acid undergoes a deoxidation reaction. However, because of the coating and decomposition of stearic acid on the surface, the content of the three metal elements (Fe, Cr, Ni) decreased.

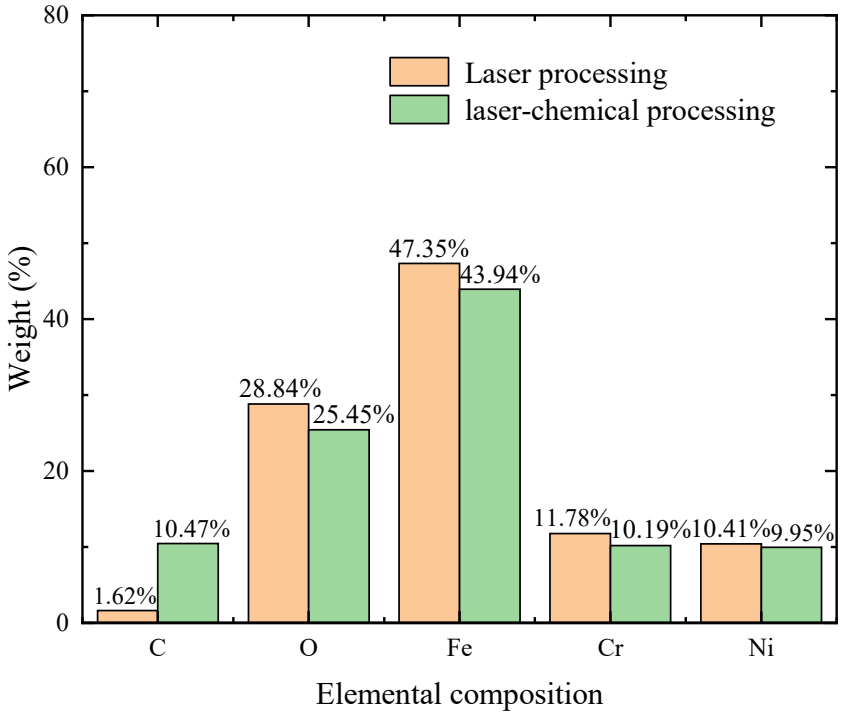

Fig. 7. EDS composition for specimen under different method

Decomposition of stearic acid by laser pulse heat leads to the occurrence of hydrodeoxygenation reaction. During Step 3, different reaction products such as n-pentadecane, n-hexadecane, n-heptadecane, n-octadecane and octadecanoyl are formed, of which n-heptadecane is the main product [34]. Previous research of the hydrodeoxygenation reaction mechanism of stearic acid, oleic acid and linoleic acid also reveals that n-heptadecane and its isomers are the main products [35-37]. The following is the reaction that occurs when stearic acid droplets are hydrodeoxygenated [38], which can reveal the formation mechanism of superhydrophobic surface during the laser-chemical recombination process.

N-heptadecane is the main reaction product of the decomposition of stearic acid. As shown in Eq. (1), stearic acid can be directly converted into n-heptadecane after decarboxylation or decarbonylation. Stearic acid undergoes a decarboxylation reaction to eliminate CO_2 to form n-heptadecane.

$$C_{17}H_{35}COOH \rightarrow C_{17}H_{36} + CO_2 \quad (1)$$

In addition, stearic acid can also undergo decarbonylation reaction, removing CO and water, each of which will generate heptadecene. Heptadecene is subsequently hydrogenated to n-heptadecane. The thermal effect of the laser accelerates the decarboxylation and decarbonylation reactions. The reaction details are shown in Eq. (2) and (3).

$$C_{17}H_{35}COOH \rightarrow C_{15}H_{31}CH{=}CH_2 + CO + H_2O \quad (2)$$

$$C_{15}H_{31}CH{=}CH_2 + H_2 \rightarrow C_{17}H_{36} + CO_2 \quad (3)$$

Several other reactions occur when stearic acid breaks down. As shown in Eq. (4), stearic acid can be catalytically reduced by hydrogen to form stearyl enthanol.

$$C_{17}H_{35}COOH + 2H_2 \rightarrow C_{18}H_{37}OH + H_2O \quad (4)$$

The stearyl enthanol produced by the catalytic reduction of stearic acid undergoes further chemical conversion through different ways. In the first approach, stearyl enthanol undergoes dehydrogenation to generate the corresponding aldehyde, and then undergoes decarbonylation reaction to eliminate CO to form n-heptadecane [39], the reaction details are shown in Eq. (5). In the second route, stearyl enthanol undergoes dehydration to produce octadecene, which is then hydrogenated to produce n-octadecane[40], as shown in Eq (6).

$$C_{18}H_{37}OH \rightarrow C_{17}H_{36} + CO + H_2 \quad (5)$$

$$C_{18}H_{37}OH + H_2 \rightarrow C_{18}H_{38} + H_2O \quad (6)$$

The formation of n-pentadecane and n-hexadecane was inferred from the reaction intermediate stearyl enthanol.

$$C_{18}H_{37}OH + 3H_2 \rightarrow C_{15}H_{32} + C_3H_8 + H_2O \quad (7)$$

$$C_{18}H_{37}OH + 2H_2 \rightarrow C_{16}H_{34} + C_2H_6 + H_2O \quad (8)$$

Under the influence of the laser thermal effect, stearic acid can also be carbonized, and the resulting carbon may also have a series of reactions with metals and metal oxides on the surface.

$$C + Fe_2O_3 \rightarrow Fe + CO_2 \quad (9)$$

$$C + Cr_2O_3 \rightarrow Cr + CO \quad (10)$$

$$C + Fe \rightarrow Fe_3C \quad (11)$$

$$C + Cr \rightarrow Cr_3C_2 \quad (12)$$

The decomposition of stearic acid produces n-pentadecane, n-hexadecane, n-heptadecane and n-octadecane, etc., all of which are substances with low surface energy and are composed of C-C(H) bonds. Due to the limitations of EDS analysis techniques, the changes in the content of carbon and oxygen elements can only be analyzed qualitatively. To reveal the formation mechanism of superhydrophobicity by laser-chemical process more clearly, the chemical composition of four as-prepared superhydrophobic surfaces were examined using XPS. Table 6 listed the manufacture process and its contact angle respectively. As shown in Fig. 8, the XPS spectra of Specimen C (Laser-chemical processing surface) contained four elements: the C 1s at 284 eV, O 1s at 530 eV, Cr 2p at 577 eV and Fe 2p at 711 eV. The content of other elements is very low, and the influence is negligible.

Table 6 Five different specimens and its contact angles

Specimen	Manufacturing process	Contact angle
A	Polished surface	69.9°
B	Laser-chemical method (L6)	103.5°
C	Laser-chemical method (W3)	153.9°
D	Stearic acid coated after laser ablation (without Step 3)	157.0°

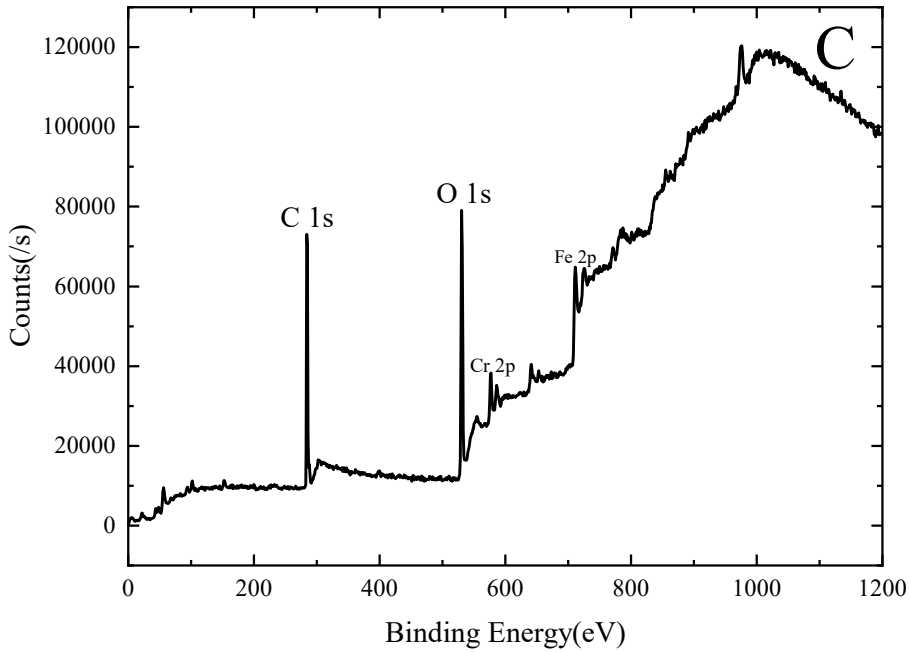

Fig. 8. XPS spectra of specimen C.

Fig. 9 (a) shows the XPS spectra of the four specimens in the binding energy range of 0 to 900 eV. Fig. 9 (b) shows the change in carbon atomic content relative to iron atomic content on the surface, expressed as the atomic C/Fe ratio. When stearic acid and its decomposition products are deposited on the stainless steel surface, less iron and more carbon were detected because the depth of analysis by XPS was only a few nanometers [41]. This results in a significant increase in the C/Fe ratio. Therefore, the C/Fe value can be used to measure the relative amount of deposited organic compounds. It can be seen that after the laser-chemical processing, the C/Fe ratio increases significantly, and the larger the C/Fe ratio, the larger the contact angle. This shows that the increase of carbon content is beneficial to increase the surface contact angle. Therefore, we believe that the increase in the contact angle of the stainless steel surface is caused by the adsorption of stearic acid and its decomposition products.

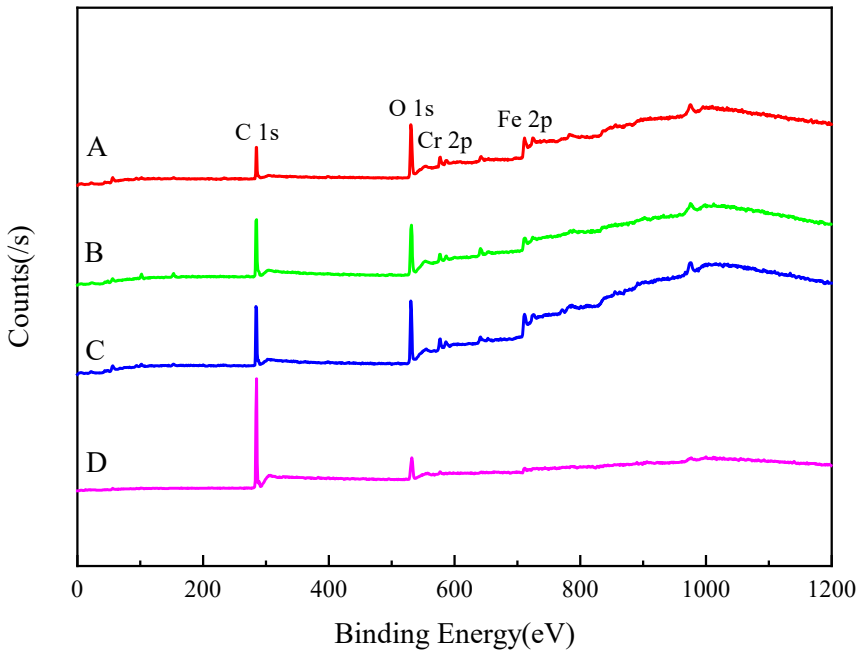

(a) XPS spectra over the binding energy range from 0 to 900 eV for different specimens.

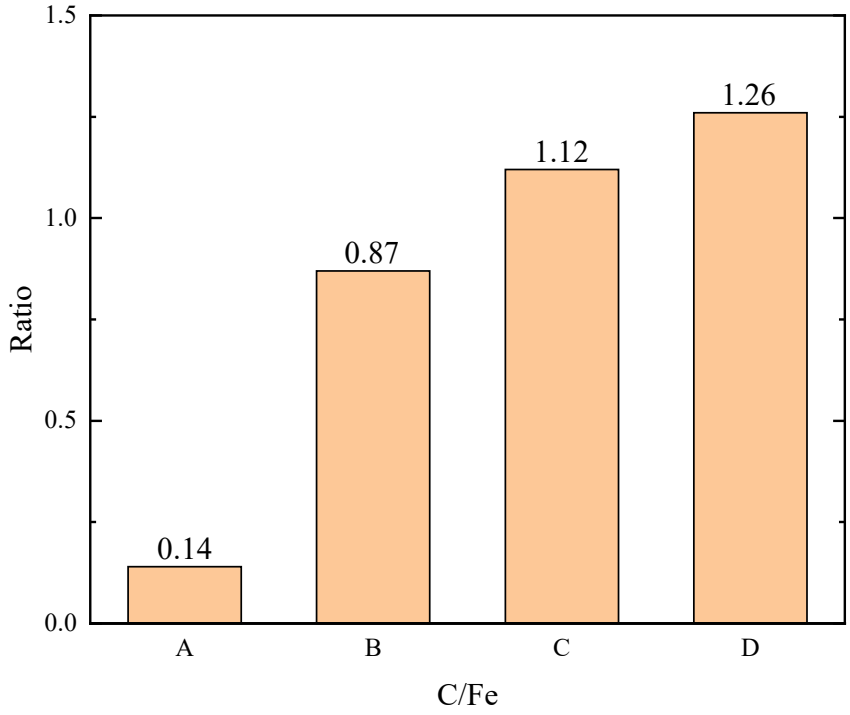

(b) The atomic C/Fe ratio on the different surface obtained from XPS spectra.

Fig. 9. XPS spectra (a) and the atomic C/Fe ratio (b) for different specimens

The C 1s peak were decomposed to further analyze the chemical state of carbon on the surface of these specimens. A fitting procedure as Ref [41] was conducted. Within each core layer, the FWHM of all peaks is constrained to be equal. The shape of all peaks is set as Gaussian curve. As shown in Fig.10 (a)-(d), the C 1s peak is fitted with four contributions, a main peak at 284.8 eV was attributed to C-C(H) bond. The

other three peaks are represent C-O, C=O and COO^- bonds. All C-O, C=O and COO^- contributions are fixed at 0.6-0.7 eV, 1.6-1.7 eV and 3.7-3.8 eV from the C-C(H) components, respectively.

In order to display these changes more clearly, the relative atomic percentages of C-C(H) bonds present on the specimens, are summarized in Fig. 10 (e). The C-C(H) is a nonpolar hydrophobic bond [42-44]. Therefore, the increase of relative content of C-C(H) bonds represents the improvement of hydrophobicity. Since the surface of specimen D is coated with stearic acid, and the C-C(H) on the surfaces of B and C are both formed by the rupture of the long chain of stearic acid. Hence, Specimen D has the greatest relative content of C-C(H) bond (82.09%). Moreover, the relative content of C-C(H) bonds on the surface of specimens B, C, and D is significantly greater than that of smooth surface A, and is directly proportional to the hydrophobicity. This further illustrates the influence of C-C(H) on surface hydrophobic properties: the more C-C(H) content, the better hydrophobicity.

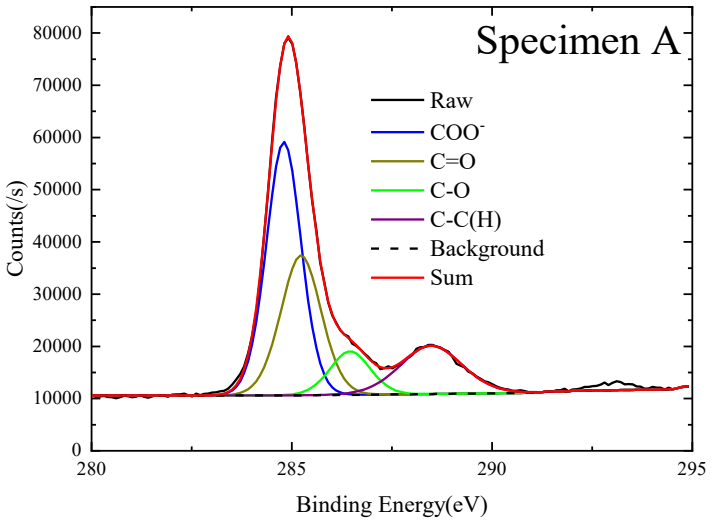

(a) Deconvolution of the XPS C 1s peaks on specimen A

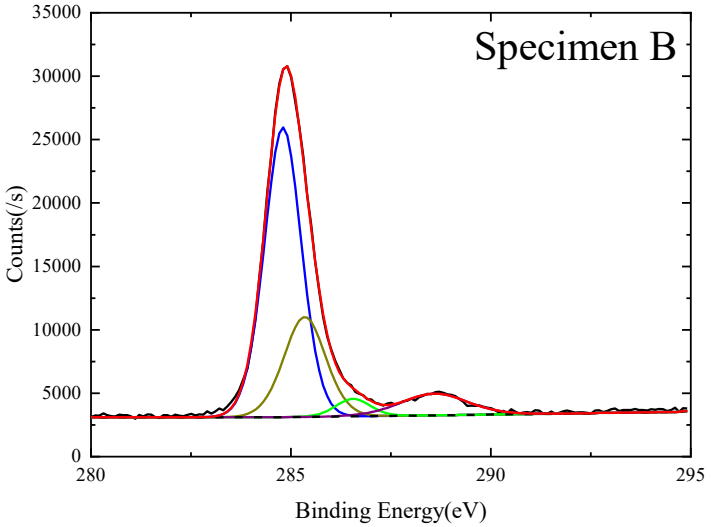

(b) Deconvolution of the XPS C 1s peaks on specimen B

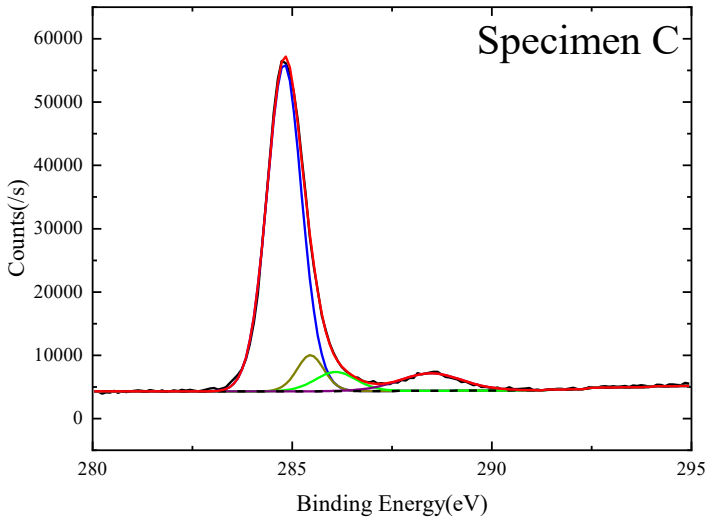

(c) Deconvolution of the XPS C 1s peaks on specimen C

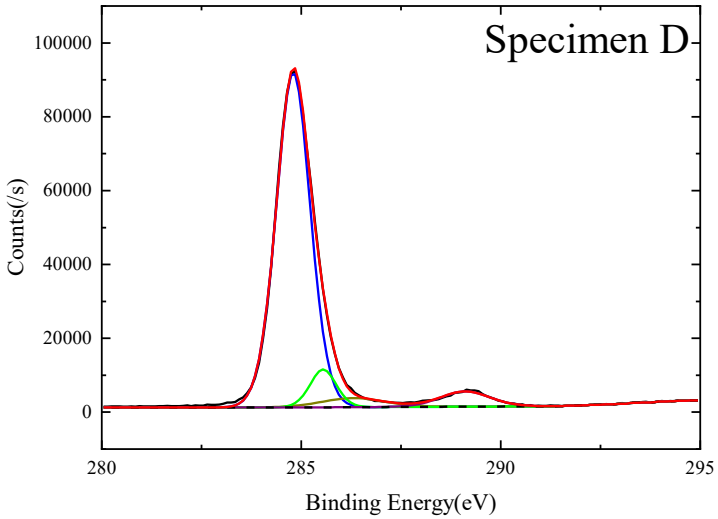

(d) Deconvolution of the XPS C 1s peaks on specimen D

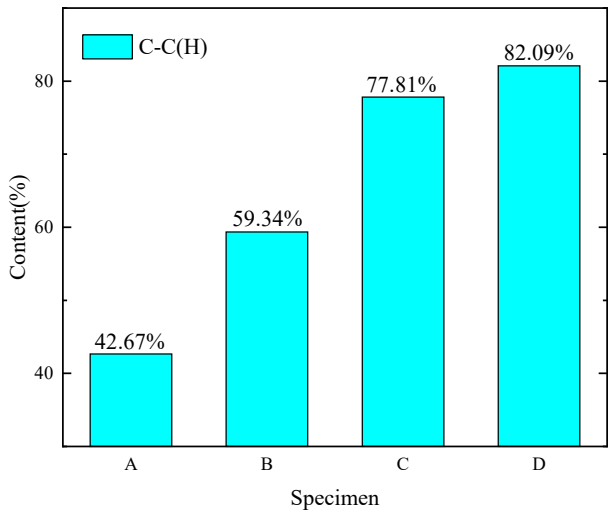

(e) Relative content of C-C(H) functional groups on different specimens

Fig. 10. Deconvolution of the XPS C 1s peaks (a)-(d) and relative content of C-C(H) functional groups (e) on different specimens

3.4 Surface chemical stability and corrosion resistance

To verify the chemical stability of the superhydrophobic surfaces prepared by laser-chemical process, three different surfaces (Group A, C and D in Table 6) mentioned above are selected for ultrasonic cleaning in enthanol and acetone. The ultrasonic cleaning temperature is 25 °C, and the ultrasonic frequency is 40 kHz. Fig. 11 compares the changes in the contact angle of three different specimens before and after 10 minutes of ultrasonic cleaning. It can be seen from the figure that the contact angle of the stearic acid coated surface is reduced from 157.0° to 105.3° before and after cleaning, while the contact angle of the laser-chemical processed surface is only reduced by 3.7°. Hence, the laser-chemical processed surface has better stability for organic solvent cleaning. The reason is that the long-chain alkane product produced by the decomposition of stearic acid has stronger surface adsorption and display better chemical stability than stearic acid. It also proved that the decomposed C-C(H) bond has stronger bond force with substrate. Lastly, it proves the necessity of Step 3 in the laser-chemical processing.

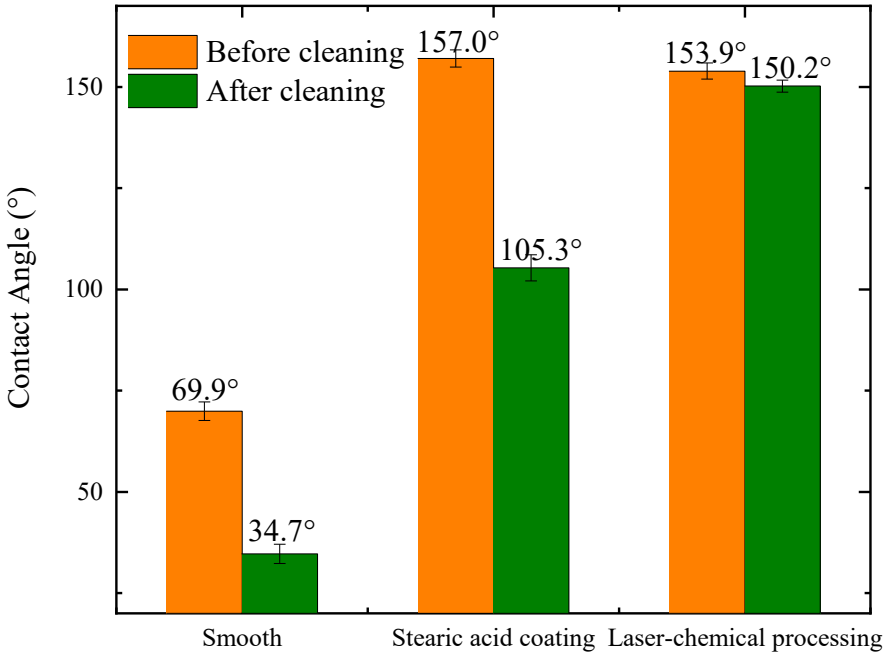

Fig. 11. Comparison of contact angle before and after ultrasonic cleaning in enthanol and acetone

The superhydrophobic surface has the effect of enhancing the corrosion resistance of metal surfaces. The 3.5 wt% NaCl aqueous solution was placed at a constant temperature of 25 °C, and the specimens A, C, and D were subjected to the dynamic point polarization curve test (PDP) by using an electrochemical workstation. During the test, a saturated calomel electrode (SCE), a platinum electrode, and a specimen with an exposed area of 1 cm^2 were used as reference electrode, counter electrode, and

working electrode, respectively. Before the PDP test, the specimens were immersed in a 3.5 wt% NaCl aqueous solution for 30 min to obtain a relatively stable open circuit potential (OCP). The PDP test was performed over a voltage range relative to OCP ±1 V with a voltage sweep rate of 1 mV/s. To ensure reproducibility of real data, all electrochemical experiments were performed at least three times.

Figure 12 plots the results of the PDP curves for the three specimens. According to Tafel extrapolation theory, the abscissa and ordinate of the intersection of the anode fitting line and the cathode fitting line represent the corrosion current density (I_{corr}) and corrosion potential (E_{corr}). The fitting results of PDP curves were also shown in Table 7. The higher E_{corr} and lower I_{corr} represent the better corrosion resistance. It can be clearly seen that the laser-chemical processing surface has a minimum I_{corr} (2.19×10^{-8} A/cm^2). It is an order of magnitude lower than the stearic acid coated surface (3.32×10^{-7} A/cm^2) and two orders of magnitude lower than smooth surface (1.55×10^{-6} A/cm^2). The laser-chemical processing surface has a higher E_{corr} (-0.016 V) than that of the stearic acid coating surface (-0.240 V) and smooth surface (-0.420 V). In order to further compare the corrosion resistance of the specimen surface, the corrosion rate (CR) is introduced by the Eq. (13) [45]:

$$CR = \frac{3.27\times10^{3}\times I_{corr}\times E}{\rho} \tag{13}$$

When I_{corr}, E and ρ represent the corrosion current density(A/cm^2), equivalent weight (g/equivalent) and density (g/cm^3) of tested substrates, respectively. The calculated corrosion rate (CR) value complied with the following sequence: Laser-chemical processing surface (2.63×10^{-4} mm/y) < Stearic acid coating surface (3.98×10^{-3} mm/y) < Smooth surface (1.86×10^{-2} mm/y). The corrosion rate of the stainless steel surface prepared by the laser-chemical processing is an order of magnitude lower than that of Rafieazad's study (5×10^{-3} mm/y) [46]. Moreover, the inhibition efficiency (η_{IE}) can be calculated by the Eq. (14).

$$\eta_{IE} = \frac{I_0 - I_c}{I_0} \tag{14}$$

Where I_0 and I_c are the corrosion current density of bare and processed 316L stainless steel, respectively. The inhibition efficiencies of laser-chemical processing and stearic acid coating are 98.6% and 78.6%. Since stearic acid is decomposed into C-C(H) bonds, the bonding strength to the substrate is greater than that of stearic acid coated on the surface, resulting in enhanced corrosion resistance. Therefore, it can be considered that the laser-chemical processing surface can significantly improve the corrosion resistance of 316L stainless steel, The method can prepare a superhydrophobic surface with good corrosion resistance on a large-area surface at low cost and is significant for the promotion and application in the industrial field.

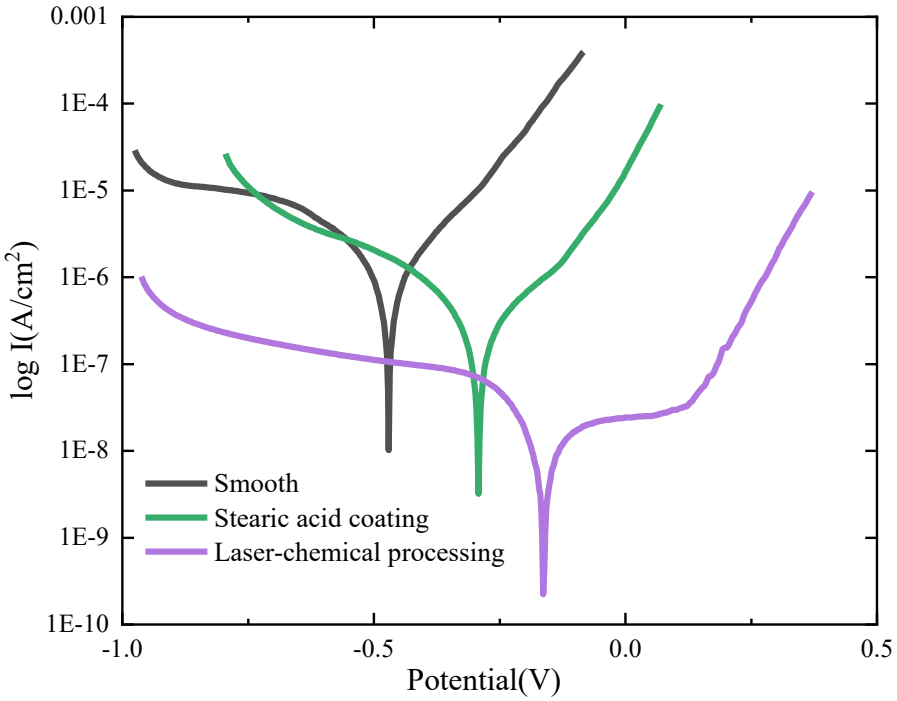

Fig. 12. PDP curves of different surfaces

Table 7 Fitting results of the polarization curves.

Manufacture Process	E_{corr}(V)	I_{corr}(A/cm^2)	CR(mm/y)	η_{IE}(%)
Smooth	-0.420	1.55×10^{-6}	1.86×10^{-2}	-
Stearic acid coating	-0.240	3.32×10^{-7}	3.98×10^{-3}	78.6
Laser-chemical processing	-0.016	2.19×10^{-8}	2.63×10^{-4}	98.6

Figure 13 is a schematic diagram of the corrosion resistance mechanism on superhydrophobic surfaces. When the stainless steel substrate is immersed in the NaCl solution, the Cl^- and water molecules are directly contact with the surface, which accelerates the corrosion process and the corrosion rate. The superhydrophobic surfaces prepared by the laser-chemical processing have micro-nano structures, which can trap air and form air pockets between the hierarchical structures [47]. It can effectively prevent water molecules and Cl^- from penetrating into the surface of the substrate, and improve the corrosion resistance of the surface.

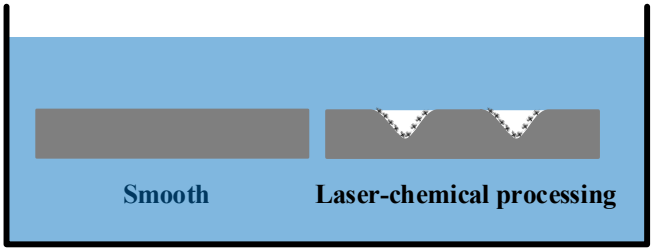

Fig. 13. Schematic diagram of corrosion resistance mechanism

4. Conclusions

In this paper, a superhydrophobic surface was successfully prepared on 316L stainless steel by a hybrid laser-chemical method. The method is simple, low-cost,

environmentally friendly, which does not require toxic chemicals or complicated instruments, and can integrate three-step processing procedures on one laser processing equipment with only one workpiece clamping. The effect of laser ablation parameters and surface pattern on hydrophobicity are investigated. Moreover, the surface chemical composition and formation mechanism of superhydrophobicity are analyzed. The conclusions are as follows.

(1) The mapping relationship between the laser ablation parameters and superhydrophobicity is established. In particular, Step 3 should choose a smaller laser power to realize thermal decomposition of stearic acid and the reduction of surface energy. Laser structuring parameters: 10 W, 150 kHz, 20 mm/s. Laser assisted decomposition of stearic acid: 1 W, 150 kHz, 50 mm/s.

(2) The effect of surface pattern and spacing on hydrophobicity was studied. Under the same scanning spacing, the mesh pattern is better than the grooves, and when the spacing is 75 μm, the prepared stainless steel surface has a best superhydrophobicity with a static contact angle of 153.9°.

(3) Normally, laser ablated stainless steel surface is superhydrophilic. However, when the hybrid laser-chemical process is completed, the surface can immediately obtain super-hydrophobicity. The major reason is the laser thermal effect promotes the hydrodeoxygenation reaction of stearic acid, and the resulting long-chain alkane product can be better bonded to the substrate. These productions have low surface energy and compose of C-C(H) bonds. The C-C(H) content is significantly increased, which improves the superhydrophobicity apparently.

(4) The long-chain alkane product produced by the decomposition of stearic acid has stronger surface adsorption and stability than stearic acid itself, which makes the superhydrophobic surface prepared by the laser-chemical processing have better durability and corrosion resistance. After ultrasonic cleaning by enthanol and acetone, the prepared surface still has good superhydrophobicity, which is not possible with ordinary coating surfaces. Moreover, the calculated corrosion rate (*CR*) value complied with the following sequence: Laser-chemical processing surface (2.63×10^{-4} mm/y) < Stearic acid coating surface (3.98×10^{-3} mm/y) < Smooth surface (1.86×10^{-2} mm/y). Hence, the laser-chemical processing surface can significantly improve the corrosion resistance of 316L stainless steel.

Acknowledgements

The authors would like to acknowledge the financial support from Guangdong Basic and Applied Basic Research Foundation (2019A1515110553), Natural Science Foundation of Shandong Province (ZR2020QE185). This work was also supported by Project for Scientific Research Innovation Team of Young Scholar in Colleges and Universities of Shandong Province (2020KJB001). This paper also supported by Key Laboratory of High-efficiency and Clean Mechanical Manufacture at Shandong University, Ministry of Education.

References

[1] Zhu K, Zhang J, Zhang H, et al. Fabrication of durable superhydrophobic coatings based on a novel branched fluorinated epoxy. Chemical Engineering Journal. 351 (2018) 569-578.

[2] Huo J, Yong J, Chen, F, et al. Xun Trapped Air-Induced Reversible Transition between Underwater Superaerophilicity and Superaerophobicity on the Femtosecond Laser-Ablated Superhydrophobic PTFE Surfaces. Advanced Materials Interfaces, 6(17) (2019) 1900262.

[3] Jokinen V, Kankuri E, Hoshian S, et al. Superhydrophobic blood‐repellent surfaces. Advanced Materials. 30 (24) (2018) 1705104.

[4] Wang L, Huang X, Wang D, et al. Lotus leaf inspired superhydrophobic rubber composites for temperature stable piezoresistive sensors with ultrahigh compressibility and linear working range. Chemical Engineering Journal. 405 (2021) 127025.

[5] Zhang B, Duan J, Huang Y, et al. Double layered superhydrophobic PDMS-Candle soot coating with durable corrosion resistance and thermal-mechanical robustness. Journal of Materials Science & Technology. 71 (2021) 1-11.

[6] Li X, Gao Z, Li B, et al. Self-healing superhydrophobic conductive coatings for self-cleaning and humidity-insensitive hydrogen sensors. Chemical Engineering Journal. 410 (2021) 128353.

[7] Wan Y, Xi C, Yu H. Fabrication of self-cleaning superhydrophobic surface on stainless steel by nanosecond laser. Materials Research Express. 5 (2018) 115002.

[8] Xiang T, Lv Z, Wei F, et al. Superhydrophobic civil engineering materials: A review from recent developments. Coatings. 9 (11) (2019) 753.

[9] Hazra A, Bonakala S, Adalikwu S A, et al. Fluorocarbon-Functionalized Superhydrophobic Metal–Organic Framework: Enhanced CO2 Uptake via Photoinduced Postsynthetic Modification. Inorganic Chemistry. 60 (6) (2021) 3823-3833.

[10] Xiang T, Han Y, Guo Z, et al. Fabrication of inherent anticorrosion superhydrophobic surfaces on metals. ACS Sustainable Chemistry & Engineering. 6 (2018) 5598-5606.

[11] Wang H, Dong S, Wang Z. One-step fabrication of superhydrophobic surface on beryllium copper alloys and corrosion protection application. Colloids and Surfaces A: Physicochemical and Engineering Aspects. 556 (2018) 291-298.

[12] Li B, Ouyang Y, Haider Z, et al. One-step electrochemical deposition leading to superhydrophobic matrix for inhibiting abiotic and microbiologically influenced corrosion of Cu in seawater environment. Colloids and Surfaces A: Physicochemical and Engineering Aspects. 616 (2021) 126337.

[13] Orazbayev S, Zhumadilov R, Zhunisbekov A, et al. Superhydrophobic carbonous surfaces production by PECVD methods. Applied Surface Science. 515 (2020) 146050.

[14] Megaraj M, Vellaisamy D K, Ramalingam D V. Fabrication and investigation of superhydrophobic surface by dip coating. Indian Journal of Chemical Technology (IJCT). 27 (1) (2020) 60-66.

[15] Long J, Pan L, Fan P, et al. Cassie-state stability of metallic superhydrophobic surfaces with various micro/nanostructures produced by a femtosecond laser. Langmuir. 32 (4) (2016) 1065-1072.

[16] Ngo C V, Chun D M. Controlling the wetting properties of superhydrophobic titanium surface fabricated by UV nanosecond-pulsed laser and heat treatment. Nanomaterials. 8 (10) (2018) 766.

[17] Ngo C V, Chun D M. Effect of Heat Treatment Temperature on the Wettability Transition from Hydrophilic to Superhydrophobic on Laser‐Ablated Metallic Surfaces. Advanced Engineering Materials. 20 (7) (2018) 1701086.

[18] Chun D M, Ngo C V, Lee K M. Fast fabrication of superhydrophobic metallic surface using nanosecond laser texturing and low-temperature annealing. CIRP Annals. 65 (1) (2016) 519-522.

[19] Ngo C V, Chun D M. Fast wettability transition from hydrophilic to superhydrophobic laser-textured stainless steel surfaces under low-temperature annealing. Applied Surface Science. 409 (2017) 232-240.

[20] Vanithakumari S C, Kumar C A, Thinaharan C, et al. Laser patterned titanium surfaces with superior antibiofouling, superhydrophobicity, self-cleaning and durability: Role of line spacing. Surface and Coatings Technology. 418 (2021) 127257.

[21] Dunn A, Wasley T J, Li J, et al. Laser textured superhydrophobic surfaces and their applications for homogeneous spot deposition. Applied Surface Science. 365 (2016) 153-159.

[22] Yang Z, Liu X, Tian Y. Insights into the wettability transition of nanosecond laser ablated surface under ambient air exposure. Journal of colloid and interface science. 533 (2019) 268-277.

[23] Yang Z, Tian Y, Zhao Y, et al. Study on the fabrication of super-hydrophobic surface on Inconel alloy via nanosecond laser ablation. Materials. 12 (2) (2019) 278.

[24] Kam D H, Bhattacharya S, Mazumder J. Control of the wetting properties of an AISI 316L stainless steel surface by femtosecond laser-induced surface modification. Journal of micromechanics and microengineering. 22 (10) (2012) 105019.

[25] Moradi S, Kamal S, Englezos P, et al. Femtosecond laser irradiation of metallic surfaces: effects of laser parameters on superhydrophobicity. Nanotechnology. 24 (41) (2013) 415302.

[26] Jagdheesh R, Pathiraj B, Karatay E, et al. Laser-induced nanoscale superhydrophobic structures on metal surfaces. Langmuir. 27 (13) (2011) 8464-8469.

[27] Bai X, Yang Q, Fang Y, et al. Anisotropic, adhesion-switchable, and thermal-

responsive superhydrophobicity on the femtosecond laser-structured shape-memory polymer for droplet manipulation. Chemical Engineering Journal. 400 (2020) 125930.

[28] Yao Lu, YanChao Guan, et al. Nanosecond laser fabrication of superhydrophobic surface on 316L stainless steel and corrosion protection application. Colloids and Surfaces A. 604 (2020) 125259.

[29] Qian W, Hua Y, Chen R, et al. Fabrication of superhydrophobic nickel-aluminum bronzes using picosecond laser for enhancing anti-corrosion property. Materials Letters. 268 (2020) 127570.

[30] LRD Lara, et al. Corrosion resistance of laser patterned ultrahydrophobic aluminium surface. Materials Letters. 184 (2016) 100-103.

[31] Ludmila, et al. Combination of Functional Nanoengineering and Nanosecond Laser Texturing for Design of Superhydrophobic Aluminum Alloy with Exceptional Mechanical and Chemical Properties. ACS Nano. 11 (10) (2017).

[32] He H, N Qu, and Y. Zeng. Lotus-leaf-like microstructures on tungsten surface induced by one-step nanosecond laser irradiation. Surface & Coatings Technology. 307 (2016) 898-907.

[33] Cai Y, et al. Superhydrophobic structures on 316L stainless steel surfaces machined by nanosecond pulsed laser. Precision Engineering. 52 (2018).

[34] Kawamura H, Ohfuji H. Nano-polycrystalline diamond synthesized through the decomposition of stearic acid. High Pressure Research. 40 (1) (2020) 162-174.

[35] Monnier J, Sulimma H, Dalai A, et al. Hydrodeoxygenation of oleic acid and canola oil over alumina-supported metal nitrides. Applied Catalysis A: General. 382 (2) (2010) 176-180.

[36] Immer J G, Kelly M J, Lamb H H. Catalytic reaction pathways in liquid-phase deoxygenation of C18 free fatty acids. Applied Catalysis A: General. 375 (1) (2010) 134-139.

[37] Berenblyum A S, Podoplelova T A, Shamsiev R S, et al. On the mechanism of catalytic conversion of fatty acids into hydrocarbons in the presence of palladium catalysts on alumina. Petroleum Chemistry. 51 (5) (2011) 336-341.

[38] KUMAR P, YENUMALA S R, MAITY S K, et al. Kinetics of hydrodeoxygenation of stearic acid using supported nickel catalysts: Effects of supports. Applied Catalysis A-general. 471 (2014) 28-38.

[39] Peng B, Zhao C, Mejía-Centeno I, et al. Comparison of kinetics and reaction pathways for hydrodeoxygenation of C3 alcohols on Pt/Al2O3. Catalysis Today. 183 (1) (2012) 3-9.

[40] Ryymin E M, Honkela M L, Viljava T R, et al. Insight to sulfur species in the hydrodeoxygenation of aliphatic esters over sulfided NiMo/γ-Al2O3 catalyst. Applied Catalysis A: General. 358 (1) (2009) 42-48.

[41] Long J Y, Zhong M L, Zhang H J, et al. Superhydrophilicity to superhydrophobicity transition of picosecond laser microstructured aluminum in ambient air. Journal of colloid and interface science. 441 (2015) 1-9.

[42] Lai J, Sunderland B, Xue J, et al. Study on hydrophilicity of polymer surfaces improved by plasma treatment. Applied Surface Science. 252 (10) (2006) 3375-3379.

[43] Pandiyaraj K N, Selvarajan V, Deshmukh R R, et al. Modification of surface properties of polypropylene (PP) film using DC glow discharge air plasma. Applied Surface Science. 255 (7) (2009) 3965-3971.

[44] Cui N Y, Brown N M D. Modification of the surface properties of a polypropylene (PP) film using an air dielectric barrier discharge plasma. Applied surface science. 189 (1-2) (2002) 31-38.

[45] KHARA S, CHOUDHARY S, SANGAL S, et al. Corrosion resistant Cr-coating on mild steel by powder roll bonding. Surface & Coatings Technology. 296 (2016) 203-210.

[46] Rafieazad M, Jaffer J A, Cui C, et al. Nanosecond laser fabrication of hydrophobic stainless steel surfaces: The impact on microstructure and corrosion resistance. Materials. 11 (9) (2018) 1577.

[47] Wang M, Zhang D, Yang Z, et al. A Contrastive Investigation on the Anticorrosive Performance of Stearic Acid and Fluoroalkylsilane-Modified Superhydrophobic Surface in Salt, Alkali, and Acid Solution. Langmuir. 36 (34) (2020) 10279-10292.